AGU PUBLICATIONS

Geophysical Research Letters

RESEARCH LETTER
10.1002/2015GL064426

Key Points:
- Electrical resistivity images of the Lastrarria volcano
- The magmatic source is located to the south of Lastarria volcano
- Deep conductor in the back arc suggests magmatic intrusion

Supporting Information:
- Readme
- Text S1
- Figure S1
- Figure S2
- Figure S3
- Figure S4

Correspondence to:
D. Díaz,
ddiaz@dgf.uchile.cl

Citation:
Díaz, D., W. Heise, and F. Zamudio (2015), Three-dimensional resistivity image of the magmatic system beneath Lastarria volcano and evidence for magmatic intrusion in the back arc (northern Chile), *Geophys. Res. Lett.*, *42*, 5212–5218, doi:10.1002/2015GL064426.

Received 4 MAY 2015
Accepted 5 JUN 2015
Accepted article online 8 JUN 2015
Published online 3 JUL 2015
Corrected 10 AUG 2015

This article was corrected on 10 AUG 2015. See the end of the full text for details.

Three-dimensional resistivity image of the magmatic system beneath Lastarria volcano and evidence for magmatic intrusion in the back arc (northern Chile)

Daniel Díaz[1,2], Wiebke Heise[3], and Fernando Zamudio[1]

[1]Departamento de Geofísica, Universidad de Chile, Santiago, Chile, [2]Centro de Excelencia en Geotermia de Los Andes, Santiago, Chile, [3]GNS Science, Lower Hutt, New Zealand

Abstract Lazufre volcanic center, located in the central Andes, is recently undergoing an episode of uplift, conforming one of the most extensive deforming volcanic systems worldwide, but its magmatic system and its connection with the observed uplift are still poorly studied. Here we image the electrical resistivity structure using the magnetotelluric method in the surroundings of the Lastarria volcano, one of the most important features in the Lazufre area, to understand the nature of the magmatic plumbing, the associated fumarolic activity, and the large-scale surface deformation. Results from 3-D modeling show a conductive zone at 6 km depth south of the Lastarria volcano interpreted as the magmatic heat source which is connected to a shallower conductor beneath the volcano, showing the pathways of volcanic gasses and heated fluid. A large-scale conductive area coinciding with the area of uplift points at a magma intrusion at midcrustal depth.

1. Introduction

The central Andes, located above the Nazca-South America subduction zone, is a prime example of a volcanic province associated with convergent plate boundaries. The presently active magmatic arc in the study zone is part of the Western Cordillera, which is located between the Precordillera region (fore arc) and the southern part of the Altiplano-Puna high plateau. The location of these major units of the central Andes is shown in Figure 1.

The Central Volcanic Zone (CVZ) of the Andes (from 15°20′S, 72°30′W to 27°20′S, 69°W) comprises 50 active or potentially active volcanoes distributed along a 1500 km arc between South Peru and Chile [*Froger et al.*, 2007]. Located in the southern part of the CVZ, Lastarria is an andesitic to dacitic stratovolcano, with a summit elevation of ~5700 m, being part of a complex, N-S oriented polygenetic structure. The currently active Lastarria volcano constitutes the main and youngest structure of the system and is formed by five NW-SE aligned nested craters [*Aguilera et al.*, 2008]. The permanent fumarolic activity at Lastarria is mainly from (i) the northwesternmost craters (from crater rim and bottom) and (ii) the NW-SE trending fracture system along the NW external flank of the Lastarria edifice. An important feature of this volcanic complex is the Negriales eruptive fissure, which originated a lava field situated SW of the main volcanic structure and composed of 0.6 ± 0.3 Ma andesitic-to-dacitic lava flow succession [*Aguilera et al.*, 2012].

The Lastarria-Cordón del Azufre volcanic zone (commonly termed "Lazufre") draws the attention of the international geosciences community due to a large-scale deformation signal detected through InSAR (interferometric synthetic aperture radar) studies [*Pritchard and Simons*, 2002; *Froger et al.*, 2007; *Ruch et al.*, 2008, 2009; *Andersohn et al.*, 2009; *Ruch and Walter*, 2010]. In this volcanic zone, the Lastarria volcano shows strong and persistent fumarolic activity, but no historic eruptions have been reported. Uplift of the Lazufre volcanic zone started after 1998 and dramatically increased thereafter up to a rate of 3 cm/yr, affecting an area between 1100 km^2 [*Ruch et al.*, 2008] and 1800 km^2 [*Ruch et al.*, 2009].

In the subduction zone of the central Andes several high-conductivity zones have been detected using the magnetotelluric method [e.g., *Schilling et al.*, 1997; *Brasse and Eydam*, 2008; *Lezaeta and Brasse*, 2001; *Díaz et al.*, 2012]. These highly conductive anomalies were observed where shear zones are present and/or magmatism has recently occurred, and their most common explanations are related to the presence of fluids and/or partial melting. Fluids released from the slab facilitate partial melting at lower crustal, upper mantle depths, by reducing the melting point of the rocks [*Wyllie*, 1988; *Iwamori*, 1998; *Grove et al.*, 2012]. At shallow depths, fluids may circulate in the crust without leading to partial melting, particularly in a brittle crust which has been folded and fractured by tectonic deformation. This process results in a considerable electrical

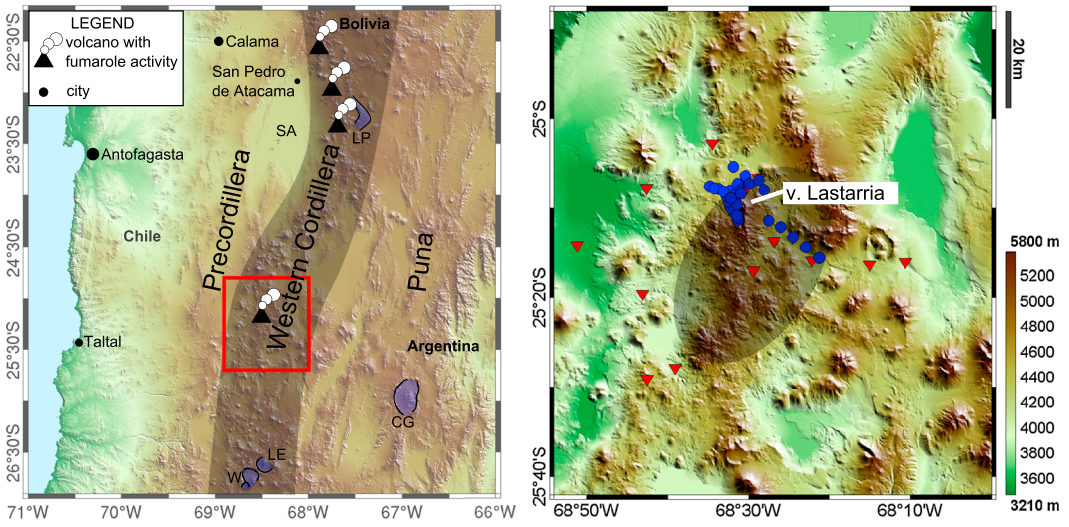

Figure 1. Study zone and location of sites. (left) The shaded zone represents the recent volcanic arc, part of the Central Andean Volcanic Zone, and including several centers of historic activity. SA is the Salar de Atacama Basin. The blue shaded zones represent some of the largest calderas in this area (CG: Cerro Galan, LE: Laguna Escondida, LP: La Pacana, W: Wheelwright [*de Silva*, 1989; *Ruch et al*., 2008]). The red rectangle corresponds to the area shown in the figure to the right. (right) Detailed view around Lastarria volcano. BBMT locations used in this work are shown in blue. Former broadband and long-period station locations are shown as red triangles [*Budach et al*., 2013]. The shaded ellipse represents the main surface deformation after *Ruch and Walter* [2010]. The color scale indicates meters above sea level.

conductivity enhancement provided that these are rich in minerals and that they find a pathway to circulate, e.g., fault zones. Hydrothermal fluids, alteration zones containing clay minerals and magmatic structures, found around active volcanic systems, are characterized by high electrical conductivity and have been identified using geophysical methods sensitive to this parameter, as magnetotellurics. Several examples can be found worldwide, where low-resistivity zones in volcanic environments have been interpreted as hydrothermal fluids [*Manzella et al*., 2004; *Ingham et al*., 2009; *Bertrand et al*., 2012] and magmatic conduits or reservoirs [*Aizawa et al*., 2008; *Ingham et al*., 2009; *Hill et al*., 2009; *Díaz et al*., 2012].

2. Magnetotelluric Data and Analysis

The magnetotelluric method measures the natural fluctuations of the Earth's electric and magnetic fields to obtain information of the resistivity distribution of the subsurface [*Chave and Jones*, 2012]. In frequency domain, the transfer function between horizontal electric (**E**) and magnetic field vector (**H**) is expressed as the complex impedance tensor **Z**, which is defined as $\mathbf{E}=\mathbf{ZH}$. Similarly, the transfer function between horizontal magnetic field components and the vertical magnetic field component (H_z) gives the induction vector *K*, defined by $H_z=\mathbf{KH}$ [*Wiese*, 1962]. In this work, real parts of the induction vectors point away from conductors (Figure 2) according to the convention of *Wiese* [1962].

The impedance tensor can be distorted by localized near-surface small-scale inhomogeneities; however, the phase relations are unaffected by these heterogeneities and provide direct information about the lateral and vertical resistivity changes at depth. We present the data therefore in the form of the phase tensor [*Caldwell et al*., 2004] which is defined as $\mathbf{\Phi}=\mathbf{X}^{-1}\mathbf{Y}$ with **X** and **Y** being the real and imaginary parts of the complex impedance tensor **Z**, respectively. The phase tensor is graphically represented by an ellipse with its principal axes (Φ_{max} and Φ_{min}, respectively). By plotting maps of phase tensor ellipses and induction vectors at different periods, main resistivity structures can be identified in the data before modeling.

Broadband magnetotelluric (BBMT) data at 30 locations in a period range of 0.001 s to 512 s were measured during field campaigns in February–March 2013 and February 2015, forming a circle around Lastarria volcano and extending as a profile to the SE, with an ~1–2 km site separation (Figure 1). The stations have been deployed in this manner trying to surround Lastarria volcano with a circular array and a profile that approaches to the maximum deformation area, always considering the difficulties to access different parts of the study area, in a very remote region of the Andes.

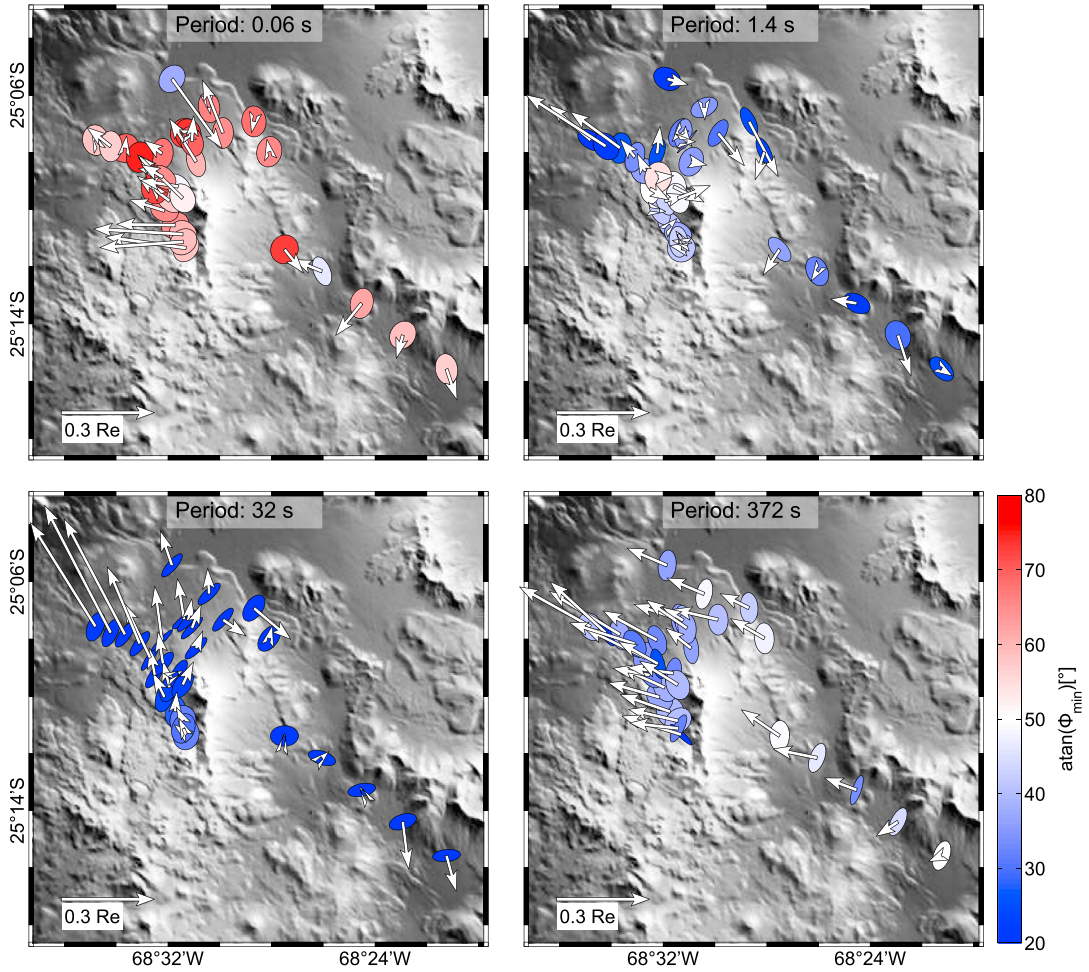

Figure 2. Induction vectors and phase tensor ellipses for periods of (a) 0.06 s, (b) 1.4 s, (c) 32 s, and (d) 372 s. Ellipses have been normalized by their major axis (Φ_{max}); the color scale shows Φ_{min}. Induction vectors point away from conductors, according to *Wiese* [1962].

Phase tensor ellipses calculated for four periods are shown in Figures 2a–2d. At very short periods, 0.06 s, the high Φ_{min} values show a near-surface conductive layer extending in a wide area around the volcano. Induction vectors indicate different directions for shorter periods and are particularly influenced by the volcanic edifice and shallow conductive structures close to the volcano. At 1.4 s high Φ_{min} values around the volcano are caused by conductive structures close to the volcanic edifice, whereas resistivity increases farther away from the volcano; large induction arrows northwest of the edifice also indicate a conductive structure close to the volcano.

At periods between 5 s and 32 s the phases are generally lower, indicating increasing resistivity at depth. However, the low Φ_{min} values and the very strong ellipticity of the sites northwest of the crater together with the large magnitude of the real induction arrows pointing northwest suggest a large deeper conductor south of the volcano.

For longer periods (e.g., 372 s), the induction arrows at the stations surrounding Lastarria volcano are aligned, pointing to a N-NW direction, and their magnitudes decrease to almost zero for the stations placed on the Puna. This behavior suggests the presence of a large-scale conductive anomaly to the southeast of the volcano, while no low-resistivity structures seem to be present directly below it at large depths.

A regional geoelectrical strike can be calculated for the whole data set using the algorithm of *Smith* [1995]. At short periods no clear strike direction can be found, while for longer periods (89 s–512 s), a regional strike of N30°E has been obtained. The 3-D nature of the data at the period ranges that define the crustal structures

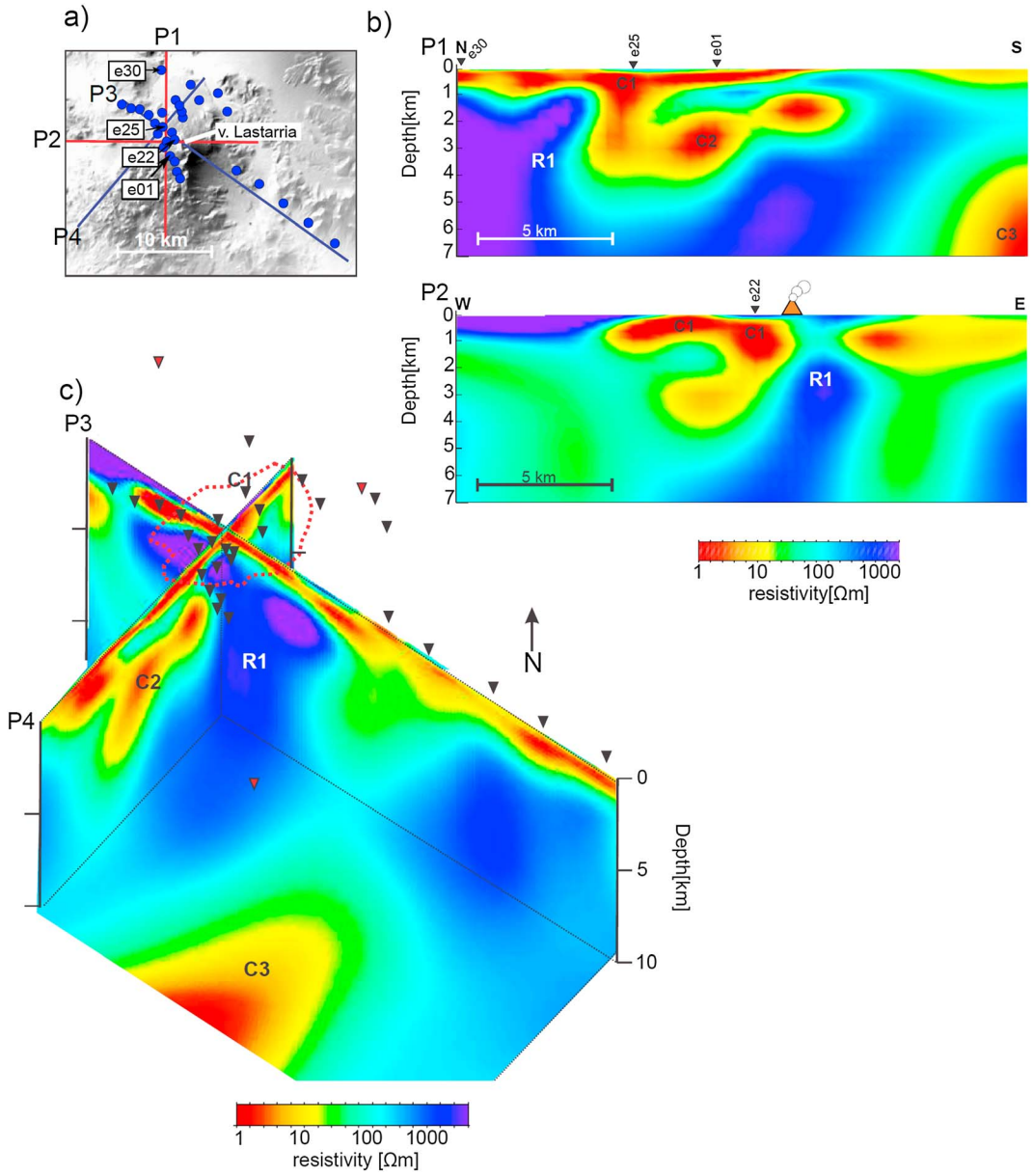

Figure 3. (a) Location map of the cross sections shown in (b) red lines and (c) blue lines. BBMT sites are marked as blue circles. (Figure 3b) NS and WE sections of the 3-D inversion model crossing Lastarria volcano. The black triangles are the broadband MT stations. (Figure 3c) NW-SE and SW-NE cross sections through the inversion model. The outline of conductive layer C1 is marked by the red dotted line.

requires a 3-D interpretation of the data. Analysis of the phase tensor skew angle β which is a measure for the asymmetry of the phase tensor shows that the data are strongly influenced by 3-D structure with very large beta values particularly in the period range between 5 s and 30 s (see Figure S1 in the supporting information).

3. Three-Dimensional Modeling

The 3-D inversion algorithm WSINV3DMT described by *Siripunvaraporn et al.* [2005] was used to model the measured data. The algorithm is based on the data space Occam's inversion and searches for a smooth model with minimum structure that fits the data to a given error level. For the 3-D case, all the elements of the impedance tensor (**Z**) are significant, and therefore, this method considers the inversion of its four components, plus two elements of the geomagnetic transfer function (for details of the inversion and

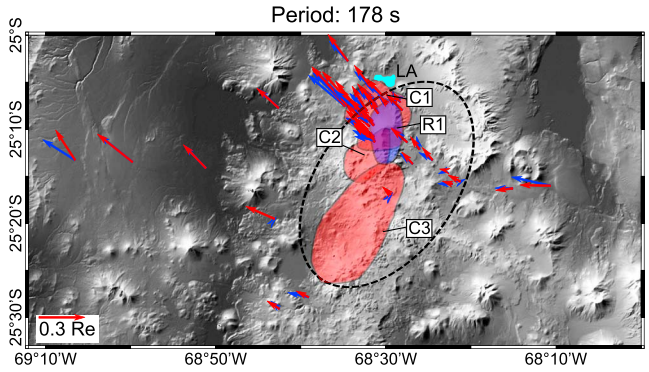

Figure 4. Real induction vectors from measured (blue) and modeled (red) data for a period of 178 s. Outlines of conductor C1, C2, and C3 are shown in red, and resistive R1 is shown in blue. Laguna Azufrera (LA) is marked in cyan. The dashed line outlines the area of uplift.

hypothesis testing, see Text S1 in the supporting information). Data at four periods per decade were used in a period range of 0.02 s and 370 s for the BBMT data and from 30 s to 3000 s for the long-period magnetotellurict (LMT) data. Topography was not included in the 3-D inversion process; however, the effect of the topography in the broadband data was tested using forward modeling (code of *Mackie et al.* [1994]) and considered not significant in the period range of interest.

The model of the BBMT data gave interesting results around the Lastarria volcano, which are well resolved until 10 km depth. In particular, the use of induction arrows in the forward modeling process showed that the presence of a large-scale conductive anomaly below 5 km depth, SE of Lastarria volcano, was necessary to fit the data for the longest periods. In order to reach larger depths and try to relate the Lastarria volcano and the Lazufre deformation source, the LMT data from *Budach et al.* [2013] were included in the 3-D inversion process, considering a broader grid reaching larger depths (see supporting information for details of the 3-D modeling).

The final model, resulting from 3-D inversion and forward modeling, shown in Figure 3 obtained a normalized RMS error of 2.8. For examples of the data fit, see Figure S2 in the supporting information. Close to the Lastarria volcanic edifice, where most of the BBMT stations were placed, the result of the 3-D inversion and hypothesis tests indicates the presence of two conductive anomalies (C1 and C2). The anomaly marked as C1 is highly conductive with values between 1 and 10 Ωm, extending down to 1 km below the surface and around the volcanic edifice (see Figures 3b and 3c). The spatial distribution of this anomaly, with highest conductivities on the western flank of Lastarria volcano, is consistent with the fumarolic activity in this area. The second conductive zone marked as C2 is located to the south of Lastarria volcano reaching 7–8 km in depth and ~5 to 10 Ωm (see Figures 3b and 3c). Conductor C2 is located mainly outside the data coverage, and therefore, the sensitivity of the data to C2 has been assessed by hypothesis testing (Figure S3 in the supporting information). Beneath the volcano from 1.5 km is a resistive (1000 Ωm) body (R1 in Figure 3), extending until 5 to 10 km in depth below the Lastarria volcano and its close surroundings.

A third conductive anomaly in the southeast (C3 in Figure 3c) was suggested by the long-period induction arrows and the LMT data available. Although the inversion model generally fits the data well, and the LMT soundings allow for better resolution at depth, the exact location of this large conductive anomaly and its shape are still difficult to resolve. Hypothesis testing (Figure S3 in the supporting information) however confirmed that conductor C3 is required by the data. The result shown in Figures 3 and 4 corresponds to a highly conductive structure (~1 Ωm) extending between 5 and 15 km (for additional sections through the inversion model, see Figure S4 in the supporting information).

4. Discussion and Conclusion

From the 3-D modeling and inversion of magnetotelluric data at and around Lastarria volcano, a conductive layer C1 beneath the summit can be identified, which is interpreted as alteration products and fluids of a hydrothermal system. This feature is in agreement with *Ruch et al.* [2009], with a very shallow source obtained through inversion of InSAR data. From geochemical analysis of thermal fluid discharges, considering isotopic composition and geothermometry, *Aguilera et al.* [2012] proposed a conceptual model for the Lastarria fumarole system. In this model, the fumarole gases are inferred to originate from magma degassing at depths between 7 and 15 km [*Froger et al.*, 2007], which constitutes the main fluid source for fumarolic vents in Lastarria area. *Aguilera et al.* [2012] suggest that two primary

fluid types are discharged: (1) superheated vapors and (2) gases produced at hydrothermal conditions by boiling of a shallow water aquifer. The alteration products (clay) and high temperatures of this boiling aquifer explain the low resistivities (~1 Ωm) that characterize conductor C1. The northern part of C1 reaches the Laguna Azufrera (see Figure 4), that could be one of the drains of the hydrothermal system of the Lastarria volcano, leaving a sulfur-rich area observed in the surface (southern part of the Laguna).

The conductive zone C2 extending to the south-southwest of Lastarria and reaching depths of 7–8 km beneath the surface is interpreted as ascending magmatic fluids which provide the heat source for the shallow hydrothermal and fumarolic system. Interestingly, C2 anomaly does not extend to the north of the volcanic edifice, but to the south, where the Negriales eruptive fissure is located, which supports its interpretation as magmatic source. A small-scale magma chamber or magmatic conduit directly below the Lastarria edifice would be difficult to resolve; therefore, the presence of this kind of structures cannot be discarded. The interpretation of C1 and C2 anomalies as hydrothermal and magmatic reservoirs shows a remarkable agreement with results of a seismic noise tomography in the Lazufre area, recently published by *Spica et al.* [2015], considering both location and extension of these features.

A rather unexpected feature is the highly resistive body R1 beneath Lastarria volcano. However, since the current magmatic system seems to be located to the south of the volcano, we suggest that the resistor is a plutonic body formed at earlier stages of the building of the volcano. This kind of resistive structures has been observed in different volcanic settings, as shown in *Aizawa et al.* [2014], where similar structures were found below the Kakuto caldera, close to currently active volcanic centers, or the resistive structures observed below Quetena volcano and Vilama caldera by *Comeau et al.* [2015]. In both cases the resistive structures were interpreted as solidified magma chambers and crystallized intrusions.

The deeper anomaly C3 is placed beneath the central part of the large-scale surface deformation area, coincident with the model suggested by *Ruch et al.* [2009], and with the upper part of the large-scale conductive anomaly suggested by *Budach et al.* [2013], using long-period MT data along a profile crossing the Lazufre area farther south of Lastarria. The shallower part of C3 has resistivities of approximately 5 Ωm at 5 km, reaching lower resistivities (0.1 Ωm) at greater depth, and it lies in the zone of maximum tensile stress proposed by *Ruch et al.* [2009]. These authors proposed a sill source at a depth of 12–14 km, in good agreement with our results. This kind of crustal magmatic reservoirs has been proposed in other large deformation areas in the Andes, such as Uturuncu volcano, where a magmatic reservoir in the lower crust is proposed [*Comeau et al.*, 2015], and in the Laguna del Maule system, where a much larger uplift rate seems to be related to a shallow magmatic reservoir [*Singer et al.*, 2014].

The presence of large-scale conductive anomalies in the back arc of the Altiplano and the Puna have been observed in several works in the central Andes [e.g., *Brasse et al.*, 2002; *Díaz et al.*, 2012; *Budach et al.*, 2013; *Comeau et al.*, 2015] and have been associated with intracrustal magma reservoirs fed by ascending partial melts. Given the coincidence with the area of uplift the interpretation of a currently forming large magmatic reservoir seems likely. However, to determine the continuation of this highly conductive anomaly below the Puna and its possible connection to the magmatic system of Lastarria volcano, more long-period MT data are needed in order to improve the data coverage in the whole area and constrain the presence of large-scale structures.

Acknowledgments

Thanks to Stefano Cararo, Sebastian Carrasco, Sebastian Del Campo, Andrea Navarro, Maximiliano Pavez, Valentina Reyes, and Luis Valdes for their support during field campaigns in 2013 and 2015. We thank H. Brasse and I. Budach from the Freie Universität Berlin, who provided the LMT data and useful suggestions for the improvement of this manuscript. W. Siripunvaraporn provided the 3-D inversion code. We thank Geodatos S.A.I.C. for providing access to a cluster and running the parallel inversion code. Most of the plots were prepared with MATLAB codes which included functions provided by F. Beauducel. This work was funded by Proyecto Fondecyt Iniciacion (11121143). We thank additional support from Centro de Excelencia en Geotermia de Los Andes, Proyecto FONDAP 15090013.

The Editor thanks Joel Ruch and an anonymous reviewer for their assistance in evaluating this paper.

References

Aguilera, F., F. Tassi, O. Vaselli, E. Medina, and T. Darrah (2008), Preliminary results of a geochemical survey at Lastarria volcano (northern Chile): Magmatic vs. hydrothermal contributions, in *7th International Symposium on Andean Geodynamics (2008: Nice, France)*, *Ext. Abstr.*, pp. 25–28, Nice, France.

Aguilera, F., F. Tassi, T. Darrah, S. Moune, and O. Vaselli (2012), Geochemical model of a magmatic hydrothermal system at the Lastarria volcano, northern Chile, *Bull. Volcanol.*, *74*, 119–134, doi:10.1007/s00445-011-0489-5.

Aizawa, K., Y. Ogawa, T. Hashimoto, T. Koyama, W. Kanda, Y. Yamaya, M. Mishina, and T. Kagiyama (2008), Shallow resistivity structure of Asama volcano and its implications for magma ascent process in the 2004 eruption, *J. Volcanol. Geotherm. Res.*, *173*, 165–177.

Aizawa, K., et al. (2014), Three-dimensional resistivity structure and magma plumbing system of the Kirishima volcanoes as inferred from broadband magnetotelluric data, *J. Geophys. Res. Solid Earth*, *119*, 198–215, doi:10.1002/2013JB010682.

Andersohn, J., M. Motagh, T. R. Walter, M. Rosenau, H. Kaufmann, and O. Oncken (2009), Surface deformation time series and source modelling for a volcanic complex system based on satellite wide swath and image mode interferometry: The Lazufre system, central Andes, *Remote Sens. Environ.*, *113*, 2062–2075.

Bertrand, E. A., et al. (2012), Magnetotelluric imaging of upper-crustal convection plumes beneath the Taupo Volcanic Zone, New Zealand, *Geophys. Res. Lett.*, *39*, L02304, doi:10.1029/2011GL050177.

Brasse, H., and D. Eydam (2008), Electrical conductivity beneath the Bolivian Orocline and its relation to subduction processes at the South American continental margin, *J. Geophys. Res.*, *113*, B07109, doi:10.1029/2007JB005142.
Brasse, H., P. Lezaeta, V. Rath, K. Schwalenberg, W. Soyer, and V. Haak (2002), The Bolivian Altiplano conductivity anomaly, *J. Geophys. Res.*, *107*(B5), 2096, doi:10.1029/2001JB000391.
Budach, I., H. Brasse, and D. Díaz (2013), Crustal-scale electrical conductivity anomaly beneath inflating Lazufre volcanic complex, central Andes, *J. South Am. Earth Sci.*, *42*, 144–149.
Caldwell, T. G., H. M. Bibby, and C. Brown (2004), The magnetotelluric phase tensor, *Geophys. J. Int.*, *158*, 457–469.
Chave, A. D., and A. G. Jones (Eds.) (2012), *The Magnetotelluric Method: Theory and Practice*, 552 pp., Cambridge Univ. Press, New York.
Comeau, M. J., M. J. Unsworth, F. Ticona, and M. Sunagua (2015), Magnetotelluric images of magma distribution beneath Volcán Uturuncu, Bolivia: Implications for magma dynamics, *Geology*, *43*, 243–246, doi:10.1130/G36258.1.
de Silva, S. L. (1989), Altiplano-Puna volcanic complex of the central Andes, *Geology*, *17*, 1102–1106.
Díaz, D., H. Brasse, and F. Ticona (2012), Conductivity distribution beneath Lascar volcano (northern Chile) and the Puna, inferred from magnetotelluric data, *J. Volcanol. Geotherm. Res.*, *217–218*, 21–29.
Froger, J. L., D. Remy, S. Bonvalot, and D. Legrand (2007), Two scales of inflation at Lastarria-Cordon del Azufre volcanic complex, central Andes, revealed from ASAR-Envisat interferometric data, *Earth Planet. Sci. Lett.*, *255*(1–2), 148–163.
Grove, T. L., C. B. Till, and M. J. Krawczynski (2012), The role of H_2O in subduction zone magmatism, *Annu. Rev. Earth Planet. Sci.*, *40*, 413–439.
Hill, G., T. G. Caldwell, W. Heise, D. G. Chertkoff, H. M. Bibby, M. K. Burgess, J. P. Cull, and R. A. F. Cas (2009), Distribution of melt beneath Mount St. Helens and Mount Adams inferred from magnetotelluric data, *Nat. Geosci.*, *2*, 785–789, doi:10.1038/NGEO661.
Ingham, M. R., H. M. Bibby, W. Heise, K. A. Jones, P. Cairns, S. Dravitzki, S. L. Bennie, T. G. Caldwell, and Y. Ogawa (2009), A magnetotelluric study of Mount Ruapehu volcano, New Zealand, *Geophys. J. Int.*, *179*, 887–904.
Iwamori, H. (1998), Transportation of H_2O and melting in subduction zones, *Earth Planet. Sci. Lett.*, *160*, 65–80.
Lezaeta, P., and H. Brasse (2001), Electrical conductivity beneath the volcanoes of the NW Argentinian Puna, *Geophys. Res. Lett.*, *28*, 4651–4654, doi:10.1029/2001GL013582.
Mackie, R. L., J. T. Smith, and T. R. Madden (1994), Three-dimensional electromagnetic modeling using unite difference equations: The magnetotelluric example, *Radio Sci.*, *29*, 923–935, doi:10.1029/94RS00326.
Manzella, A., G. Volpi, A. Zaja, and M. Meju (2004), Combined TEM-MT investigation of shallow-depth resistivity structure of Mt. Somma-Vesuvius, *J. Volcanol. Geotherm. Res.*, *131*, 19–32.
Pritchard, M. E., and M. Simons (2002), A satellite geodetic survey of large-scale deformation of volcanic centres in the central Andes, *Nature*, *418*(6894), 167–171.
Ruch, J., and T. R. Walter (2010), Relationship between the InSAR-measured uplift, the structural framework, and the present-day stress field at Lazufre volcanic area, central Andes, *Tectonophysics*, *492*, 133–140.
Ruch, J., J. Anderssohn, T. R. Walter, and M. Motagh (2008), Caldera-scale inflation of the Lazufre volcanic area, South America: Evidence from InSAR, *J. Volcanol. Geotherm. Res.*, *174*, 337–344.
Ruch, J., A. Manconi, G. Zeni, G. Solaro, A. Pepe, M. Shirzaei, T. R. Walter, and R. Lanari (2009), Different deformation scales and stress field change in the Lazufre volcanic area, central Andes, *Geophys. Res. Lett.*, *36*, L22303, doi:10.1029/2009GL041276.
Schilling, F., G. M. Partzsch, H. Brasse, and G. Schwarz (1997), Partial melting below the magmatic arc in the central Andes deduced from geoelectromagnetic field experiments and laboratory data, *Phys. Earth Planet. Inter.*, *103*, 17–31.
Singer, B. S., et al. (2014), Dynamics of a large, restless, rhyolitic magma system at Laguna del Maule, southern Andes, Chile, *GSA Today*, *24*, 4–10, doi:10.1130/GSATG216A.1.
Siripunvaraporn, W., G. Egbert, Y. Lenbury, and M. Uyeshima (2005), Three-dimensional magnetotelluric inversion: Data-space method, *Phys. Earth Planet. Inter.*, *150*, 3–14.
Smith, J. T. (1995), Understanding telluric distortion matrices, *Geophys. J. Int.*, *122*, 219–226.
Spica, Z., et al. (2015), Hydrothermal and magmatic reservoirs at Lazufre volcanic area, revealed by high-resolution seismic noise tomography, *Earth Planet. Sci. Lett.*, *421*, 27–38.
Wiese, H. (1962), Geomagnetische Tiefentellurik Teil II: Die Streichrichtung der untergrundstrukturen des elektrischen Widerstandes, erschlossen aus geomagnetischen Variationen, *Pure Appl. Geophys.*, *52*, 83–103.
Wyllie, P. J. (1988), Magma genesis, plate tectonics, and chemical differentiation of the Earth, *Rev. Geophys.*, *26*, 370–404, doi:10.1029/RG026i003p00370.

Erratum

In the originally published version of this article, Figure 2 appeared incorrectly. The error has since been corrected, and this version may be considered the authoritative version of record.